

Further Evidence for Resonant Photoelectron–Solvent Scattering in Nitrous Oxide Cluster Anions[†]

Emily R. Grumbling, Kostyantyn Pichugin, Luis Velarde,[‡] and Andrei Sanov*

Department of Chemistry and Biochemistry, University of Arizona, Tucson, Arizona 85721-0041

Received: July 16, 2009; Revised Manuscript Received: September 18, 2009

The effects of anion solvation by N₂O on photoelectron angular distributions are revisited in light of new photoelectron imaging results for the NO[−](N₂O)_{*n*}, *n* = 0–4 cluster anions at 266 nm. The new observations are examined in the context of the previous studies of O[−] and NO[−] anions solvated in the gas phase by nitrous oxide [Pichugin; et al. *J. Chem. Phys.* et al. **2008**, *129*, 044311.; Velarde; et al. *J. Chem. Phys.* et al. **2007**, *127*, 084302.]. The photoelectron angular distributions collected in the three separate studies are summarized and analyzed using bare O[−] and NO[−] as zero-solvation references. Solvent-induced deviations of the angular distributions from the zero-solvation reference are scaled by solvation number (*n*) to yield solvent-induced anisotropy differentials. These differentials, calculated identically for the O[−](N₂O)_{*n*} and NO[−](N₂O)_{*n*} cluster series, show remarkably similar energy dependences, peaking in the vicinity of a known electron–N₂O scattering resonance. The results support the conclusion that the solvation effect on the photoelectron angular distributions in these cases is primarily due to resonant interaction of photoelectrons with the N₂O solvent, rather than a solvent-induced perturbation of the parent-anion electronic wave function.

1. Introduction

Chemical structure and reactivity are dictated by electronic interactions in and between molecules. Photoelectron imaging of negative ions has proven to be a powerful tool for studying the electronic properties of chemical species in the gas phase, complementing traditional photoelectron spectroscopy.^{1,2} A single experiment yields both the photoelectron energy spectrum, from which adiabatic electron affinities and vertical detachment energies may be extracted, and energy-dependent angular distributions.^{3–5} The interpretation of photoelectron angular distributions has focused mainly on the properties of the parent-anion orbitals,^{6,7} but it is becoming apparent that they also yield insight into the environment in which the detachment process occurs, specifically by revealing solvation effects.

When photoelectron angular distributions in the photodetachment of cluster anions are interpreted, several solvent-induced effects must be considered.⁸ First, the anion–neutral solvation interaction stabilizes the electronic state of the anion more than that of the neutral, resulting in increased electron binding energies (eBE) for solvated species.^{9,10} As the partial wave contributions to the photoelectron wave function depend upon the electron’s kinetic energy (eKE), a solvation-induced shift in eBE (and, therefore, eKE) affects the angular distribution. Second, the solvent perturbs the electronic structure of the anion, possibly accommodating some of the charge.^{9,11} This perturbation of the initial state may, for example, have the effect of allowing additional partial-wave contributions to the photoelectron wave function. Third, the wave function of the photoelectron itself may be perturbed by interactions with the solvent molecules.

Several studies suggest that solvent-induced perturbation of the photoelectron has a particularly pronounced effect when the

asymptotic electron kinetic energy is in the vicinity of an anionic resonance of the solvent. In one case, 266 nm photodetachment from I[−]·CH₃I yielded photoelectrons that were markedly more isotropic than those detached from I[−]·H₂O, I[−]·Ar, or I[−]·CH₃CN.¹² This was attributed to scrambling of the nascent photoelectron angular distribution via one of several possible electron–CH₃I scattering resonances¹³ near the 1.2 eV kinetic energy of the photoelectrons in that particular measurement.¹² A similar observation was made upon comparison between detachment from anionic acetone clusters (Acn)_{*n*}[−] (*n* = 5–15) to their hydrated analogues, Acn[−](H₂O)_{*m*} (*m* = 5–10).¹⁴ In this case, the smaller anisotropies for detachment from the homogeneous clusters were attributed to an electron–acetone scattering resonance in the eKE range accessed in the experiment.

Recently, our group reported another case of dominant photoelectron–solvent interactions evidenced by photoelectron anisotropy shifts upon solvation of NO[−] by N₂O in cluster–anion photodetachment at 786, 532, and 355 nm.⁸ A fit to experimentally determined anisotropy parameters (β) for detachment from bare NO[−] using the Cooper–Zare central-potential model^{3,4} was used as a basis for comparison. To examine the effect of both eKE and *n* on the photoelectron anisotropy for the NO[−](N₂O)_{*n*} cluster anions, a new parameter (the “anisotropy differential”) was introduced, calculated as

$$D(\text{eKE}) = \frac{\beta(\text{eKE}) - \beta_{\text{CZ}}(\text{eKE})}{n^{0.8}} \quad (1)$$

where $\beta(\text{eKE})$ is the experimentally determined photoelectron anisotropy parameter for a given cluster of solvation number *n* corresponding to a transition centered at a specific eKE, while $\beta_{\text{CZ}}(\text{eKE})$ is the Cooper–Zare prediction for detachment from the core anion in the absence of solvation but at the same electron kinetic energy as the $\beta(\text{eKE})$ measurement. The exponent of 0.8 is an empirical parameter that accounts for the

[†] Part of the “W. Carl Lineberger Festschrift”.

* Corresponding author. E-mail: sanov@u.arizona.edu.

[‡] Present address: Department of Chemistry, University of California, Santa Barbara, CA 93106-9510.

nonlinear contribution of multiple solvent molecules, determined to best overlap the data sets obtained at different wavelengths.⁸

When plotted as a function of eKE, the resulting anisotropy differentials peaked at approximately the same energy as a computed momentum-transfer cross-section for electron collisions with N₂O (~2.25 eV).¹⁵ The same analysis for 355 nm detachment from NO⁻(H₂O)_n (*n* = 1–3, peak eKE = 0.9–2.13 eV) yielded a less pronounced loss of anisotropy with a different energy dependence, confirming that the effect is specific to the N₂O solvent. Since the electrostatic (solvation) interactions of NO⁻ with H₂O are stronger than with N₂O, it was concluded that the anisotropy loss is not primarily due to perturbation of the initial bound state.⁸

Most of the data in the previous work corresponded to the low-energy side of the scattering resonance implicated in the analysis. In the present work, we revisit the NO⁻(N₂O)_n cluster series at 266 nm, extending the observation range to larger electron kinetic energies. In addition, the results peripherally reveal the signature of another core anion for *n* = 1–4, assigned to the ONNNO⁻ structure first proposed by Hiraoka et al.¹⁶ and characterized spectroscopically by Continetti and co-workers.¹⁷ We examine the coexistence of the NO⁻ and ONNNO⁻ cluster cores under stepwise solvation by N₂O and interpret the findings in terms of gradual core-*shifting* (rather than abrupt core-*switching*^{18–21}) attributed to the interplay between the relative stabilities of the NO⁻ and ONNNO⁻ anions and the preferential solvation of the smaller NO⁻ core.

In the following, we present the new photoelectron imaging results and the complete set of NO⁻(N₂O)_n anisotropy parameters and differentials. These results are compared to the corresponding data from 355 and 266 nm photodetachment of O⁻(N₂O)_n, *n* = 0, 4–9. The remarkable similarities between the anisotropy differentials for the two different cluster series provide further evidence for the effect of the anionic N₂O resonance on the photoelectron angular distributions. It is hoped that these results and analyses will prompt deeper probing into the chemical significance of photoelectron imaging results for cluster anions.

2. Experimental Apparatus and Data Analysis

Experiments are performed in a negative-ion photoelectron imaging spectrometer described in detail elsewhere.⁶ The instrument combines velocity-map^{22,23} imaging^{24–26} detection of photoelectrons^{1,27} with the negative-ion techniques pioneered by Lineberger.²⁸

In brief, ions are formed in a low-pressure (10⁻⁷ Torr base, ≤10⁻⁴ Torr operational) chamber upon supersonic expansion of neat N₂O from a pulsed nozzle (General Valve Series 9) operating at 50 Hz, bombarded by a 1 keV electron beam. For enhanced production of cluster anions, the electron beam propagates counter to the expansion, into the nozzle's orifice.²⁹ Negative ions are extracted into a Wiley–McLaren³⁰ time-of-flight mass spectrometer, where they are accelerated to ~2.5 kV and focused using an Einzel lens. Ions are detected using a dual-microchannel plate detector, with the output read from a digitizing oscilloscope, yielding time-of-flight mass spectra.

Nanosecond pulses (50 Hz) of the fourth harmonic from a Nd:YAG laser (Spectra Physics Corp., model Lab 130-50), entering the detection region through a Brewster window and timed to intersect the target anions, propagate perpendicularly to the ion trajectory. Upon detachment, photoelectrons are projected by velocity-mapping electrodes onto a two-dimensional position-sensitive dual-microchannel-plate detector coupled to a phosphor screen (Burle, Inc.), allowing the amplified

photoelectron signal to be recorded with a digital camera. The detector's surface is parallel to the plane defined by the laser and ion propagation directions. The laser beam is focused with a lens (*f* = 2 m) placed approximately 1 m before the laser-ion interaction region, corresponding to a laser fluence of ~1.0 × 10⁶ W/cm² in this region. The laser polarization is linear in the direction parallel to the ion beam and the surface of the imaging MCP detector.

The zero-solvation reference NO⁻ data were collected at 266 nm by averaging ~100 000 experimental cycles. Photoelectron images for each member of the NO⁻(N₂O)_n (*n* = 1–4) cluster series at 266 nm were obtained on three separate days, expanding on the previous work.⁸ We have also supplemented our previous 266 nm data for O⁻(N₂O)_n (*n* = 0, 4–9) under the same experimental conditions,²¹ with the equivalent of two more data sets to improve the signal-to-noise ratio. For a given cluster of size *n*, images belonging to a single data set (i.e., collected on the same day) were combined and treated as a single image. Each of the three resulting images (one image per day for a given cluster) consist of 90 000 to 270 000 experimental cycles (depending on the signal-noise ratio for a given *n* in each cluster series) collected in small (15 000 cycles) batches with corresponding background subtraction. The anisotropy parameters reported here represent averages of the values derived from three separate daily data sets, with the error bars representing ±2 standard deviations. We also report the photoelectron anisotropy parameters obtained from our previous 355 nm O⁻(N₂O)_n results²¹ consisting of 3–5 images for a given *n* (analyzed individually), each corresponding to 30 000 experimental cycles.

Three-dimensional photoelectron probability distributions were reconstructed from the raw images using the BASEX program.³¹ Angular distributions were calculated over the full width at half-maximum of the O⁻-based transitions and the entire Franck–Condon envelope of the NO⁻-based transitions. The O⁻ transitions were used for energy calibration in all cases. The absolute energy resolution of the imaging technique scales as eKE^{1/2}. Under the conditions used in this study, the full widths at half-maximum for the 266 nm O⁻ detachment transitions are 145 and 243 meV, at electron kinetic energies of 1.24 and 3.18 eV, respectively.

3. Results

Photoelectron Images of [NO(N₂O)_n]⁻ (*n* = 0–4) at 266 nm. The cumulative 266 nm photoelectron images and spectra for NO⁻(N₂O)_n (*n* = 0–4) are presented in Figure 1 along with the average vertical detachment energies (VDEs) and anisotropy parameters (±2 standard deviations) for each transition. The *n* = 0 image shows limited vibrational structure which is more apparent in the magnified inset in Figure 1. The NO⁻ spectral band (labeled I) progressively shifts to higher VDEs with the addition of each solvent molecule, as expected in general along a solvation series and seen for this system previously^{8,32,33} at various other wavelengths. For *n* ≥ 1 we note a second, higher-eBE transition (labeled II), peaking parallel to the laser polarization direction in contrast to the NO⁻-based transitions. This second feature, while absent for *n* = 0, persists through *n* = 4, though its relative intensity decreases along the series. This feature is attributed to a second isomer of the *n* = 1 species. The *n* = 1 photoelectron spectrum is similar to that obtained by the Continetti group at the same wavelength, with the notable difference that their spectrum contains features consistent with photodetachment from O⁻, while ours does not. The O⁻ signal, observed by the Continetti group using a laser fluence of ~2 ×

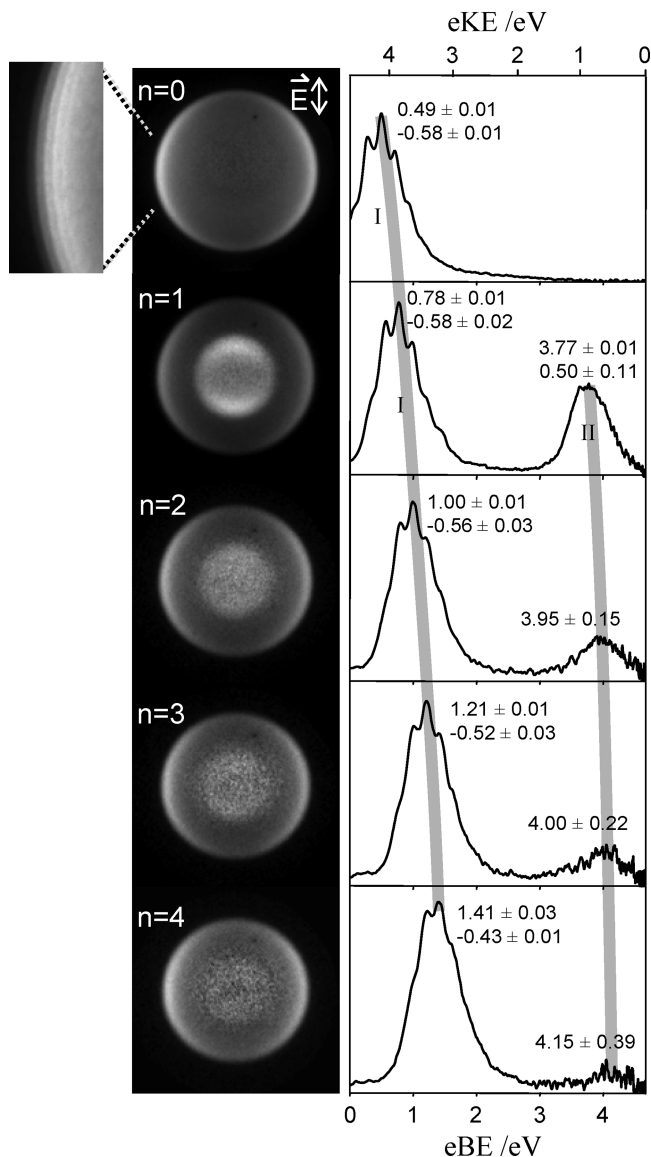


Figure 1. Photoelectron images and spectra for $\text{NO}^-(\text{N}_2\text{O})_n$, $n = 0-4$, obtained at 266 nm. Laser polarization is vertical in the plane of the page. Top and bottom values indicated for each type I band as well as band II for $n = 1$ are the peak eKEs (in eV) and anisotropy parameters (β), respectively, while only the peak eKEs are reported for $n = 2-4$ type II bands. Anisotropy parameters were determined for the angular distributions over the entire Franck–Condon envelope of each transition. The gray lines are intended to aid the eye in recognizing the shifts in VDE along the solvation series.

10^8 W/cm^2 , was attributed to photodissociation of the parent anion species, generating O^- , followed by photodetachment of the fragment with a second photon from the same laser pulse.¹⁷ In our experiment a much lower laser fluence of $\sim 1 \times 10^6 \text{ W/cm}^2$ was used. The absence of similar features in our $n = 1$ spectrum, therefore, supports the Continetti group's assignment of this feature to a two-photon process.

Photoelectron anisotropy parameters (β) were calculated over the Franck–Condon envelope of each transition. The β values for the NO^- -based transitions (band I), including bare NO^- , are plotted in Figure 2a as a function of the transition's peak eKE, along with the previous results for this cluster series at 786, 532, and 355 nm,⁸ with error bars of ± 2 standard deviations. The data point for bare NO^- at 266 nm in Figure 2a reflects the results of the new measurement only (without combining it with past data), as the present work was carried

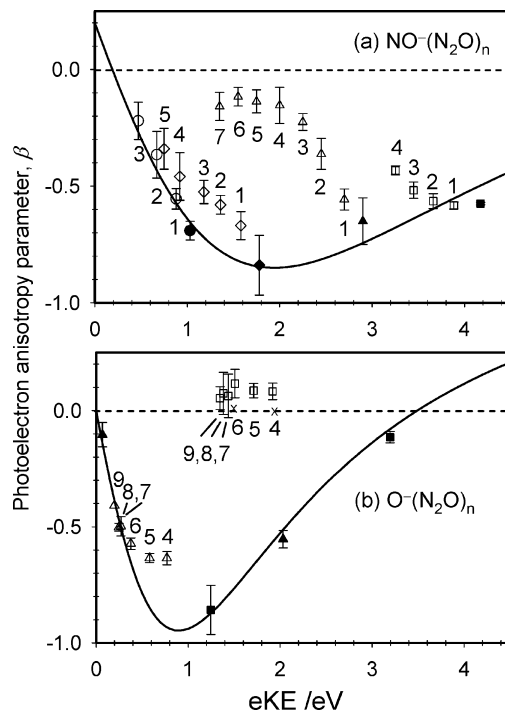


Figure 2. (a) Summary of the photoelectron anisotropy parameter (β) values for the $\text{NO}^-(\text{N}_2\text{O})_n$ cluster series plotted vs electron kinetic energy: circles, 786 nm (data from ref 8); diamonds, 532 nm (data from ref 8); triangles, 355 nm (data from ref 8); squares, 266 nm (this study). Filled symbols correspond to bare NO^- (i.e., $n = 0$), while open symbols are used to show the results for solvated clusters ($n > 0$). The integers next to the cluster data points indicate the corresponding solvation numbers n . The Cooper–Zare curve, obtained by fitting the model equation^{3–5} to the unsolvated NO^- data under the $l = 2$ approximation, is plotted as a solid line (the fit parameters are given in the text). (b) Similar summary of the photoelectron anisotropy parameter values determined for the $\text{O}^-(\text{N}_2\text{O})_n$, $n = 0, 4-9$ cluster series: triangles, 355 nm (data from ref 21); squares, 266 nm (this study). Data points corresponding to the unsolvated O^- (i.e., $n = 0$) transitions yielding both the ^3P and ^1D neutral states are included (filled symbols). The Cooper–Zare curve for O^- (see text) is also plotted as a reference.^{34,47} The \times symbols correspond to β determination for $n = 4, 6$ at 266 nm with the laser polarization direction set perpendicular to the plane of the detector (see the text for details).

out with significantly lower experimental backgrounds and greater data accumulation times (as evidenced by the excellent quality of the photoelectron image in Figure 1 for $n = 0$).

Photoelectron Anisotropies for $\text{O}^-(\text{N}_2\text{O})_n$ ($n = 4-9$) at 355 and 266 nm. Photoelectron images of $\text{O}^-(\text{N}_2\text{O})_n$ obtained at 355 and 266 nm have been reported by our group previously in the context of $\text{O}^- \leftrightarrow \text{NNO}_2^-$ core-switching in the $[\text{O}(\text{N}_2\text{O})_n]^-$ cluster series.²¹ The corresponding anisotropy parameter values for the O^- -based transitions (observed for $n = 4-9$) are plotted in Figure 2b. We reproduce these data here, because they provide a basis for comparison with the $\text{NO}^-(\text{N}_2\text{O})_n$ results. As discussed later, it is the combination of the results for two different cluster series that clearly establishes the central role of N_2O , rather than O^- or NO^- , in the observed phenomena. The 355 nm results for $\text{O}^-(\text{N}_2\text{O})_n$ in Figure 2b are taken directly from the previous work,²¹ while the 266 nm data reflect a combination of the old²¹ and new photoelectron images collected for additional signal statistics.

The $\text{O}^-(\text{N}_2\text{O})_n$ transitions analyzed correspond to the final ^3P state of solvated oxygen, while for bare O^- both the ^3P and ^1D neutral pathways are included. The Cooper–Zare curve for O^- , using the parameters of Hanstorp et al.,³⁴ is also shown in

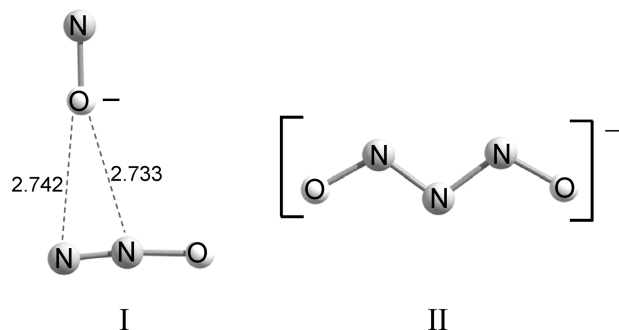


Figure 3. Structures of the $n = 1$ isomers (I) $\text{NO}^-(\text{N}_2\text{O})$ and (II) ONNNO^- , plotted to scale according to the results of the ROHF/6-31+G and RHF/6-31+G calculations, respectively, by Hiraoka et al.¹⁶ The intermolecular distances for isomer I are indicated in Angstroms. All other geometric parameters are found in Figure 9 of ref 16.

Figure 2b. In the low-eKE range, the 355 nm anisotropy parameters for the O^- -based clusters fall close to the O^- Cooper–Zare curve but deviate from it increasingly with increasing eKE. The 266 nm angular distributions (for peak eKEs between 1.35 and 1.92 eV) show stronger deviations from the Cooper–Zare curve; these transitions are nearly isotropic—in fact slightly positive—in stark contrast to the negative values of the Cooper–Zare curve for bare O^- in the corresponding energy region.

4. Discussion

Core-Shifting in $[\text{NO}(\text{N}_2\text{O})_n]^-$. Two distinct transition types, labeled bands I and II and corresponding to different core anions, are apparent in the $[\text{NO}(\text{N}_2\text{O})_n]^-$ photoelectron images and spectra in Figure 1. With each additional n , each transition is shifted to successively higher eBEs; solvation stabilizes the anion more than the corresponding neutral and thus the anion-neutral energy gap increases with increasing n . The difference between a band's VDE for anion clusters of size n and size $n - 1$ is an estimate of the stabilization of the anion cluster by addition of the n th solvent molecule. Type I transitions are assigned to photodetachment from NO^- or an N_2O -solvated NO^- core, while the higher-eBE transitions (type II) are ascribed, on the basis of the following arguments, to the ONNNO^- core anion. The structures of the two $n = 1$ isomers, (I) $\text{NO}^-(\text{N}_2\text{O})$ and (II) ONNNO^- , based on the calculated parameters reported by Hiraoka et al.,¹⁶ are shown in Figure 3.

Band II is not present for $n = 0$ but is seen for $n \geq 1$. For $n = 1$, it peaks at approximately 3.8 eV, consistent with the feature observed by Resat et al.,¹⁷ who assigned it to a w-shaped (C_{2v} symmetry) covalent ONNNO^- structure. This structure, first proposed by Hiraoka et al. (RHF/6-31+G),¹⁶ was computed by Snis and Panas [B3LYP/6-311+G(d)]³⁵ to have VDEs of 3.92 and 3.93 eV for detachment to the $^2\text{B}_2$ and $^2\text{A}_1$ states of the neutral, respectively. Both of these values are in good agreement with the observed maximum of band II.

More recently, it was proposed³⁶ that $\text{NO}_2^-(\text{N}_2)$, structurally related to the computed³⁷ cyclic intermediate of dissociative electron attachment to nitrous oxide, $\text{O}^-(\text{N}_2)$, could be responsible for this transition. While the positive β of band II is consistent with our experimental observations for detachment from unsolvated NO_2^- ,³⁸ we find the $\text{NO}_2^-\cdot\text{N}_2$ structure incompatible with the VDE reported here and in the work of Resat et al.¹⁷ The VDE for $\text{NO}_2^- (X^2\text{A}_1 \leftarrow X^1\text{A}_1)$ is ≈ 2.8 eV.^{38–41} We may estimate the VDE of $\text{NO}_2^-(\text{N}_2)$ to be only slightly greater than that of the bare ion because N_2 should interact weakly with the anion. The cyclic $\text{O}^-(\text{N}_2)$ isomer was

predicted to be stable by only 0.18 eV with respect to $\text{O}^- + \text{N}_2$,³⁷ consistent with a relatively weak electrostatic interaction; assuming a similar stabilization of NO_2^- we expect the VDE for $\text{NO}_2^-(\text{N}_2)$ to be approximately 3.0 eV, which is significantly different from the 3.8 eV value observed for transition II in Figure 1 ($n = 1$). For further comparison, we note the VDE for $\text{NO}_2^-(\text{NO})$ is ≈ 3.1 eV.⁴¹

The positive photoelectron anisotropy parameter for transition II is consistent with detachment from a totally symmetric orbital.⁷ According to the s&p approach,⁶ photodetachment from a C_{2v} symmetry molecule, such as ONNNO^- , with positive anisotropy is likely to originate from an a_1 orbital. (We caution, however, that this argument is best suited for low-eKE transitions in small, relative to the de Broglie wavelength of the photoelectron, anions.) Therefore, the properties of transition II are consistent with detachment from an a_1 orbital. Some possible contribution from b_2 orbital photodetachment could help account for the magnitude of the anisotropy parameter, consistent with the predictions of Snis and Panas for the ONNNO^- anion.³⁵

Unlike our observations for the $[\text{O}(\text{N}_2\text{O})_n]^-$, $n = 1–9$ clusters,²¹ there is no clear size-dependent core-switching between the $\text{NO}^-(\text{N}_2\text{O})_n$ and $\text{ONNNO}^-(\text{N}_2\text{O})_{n-1}$ isomers in the $[\text{NO}(\text{N}_2\text{O})_n]^-$ series. On the basis of the data in Figure 1, the two isomers coexist for all degrees of solvation examined ($n = 1–4$), and we make two additional observations regarding their coexistence.

First, the successive solvation-induced shifts in peak eBE for isomer II are consistently smaller than those for isomer I throughout the cluster series. This is easily seen upon examination of the differing slopes of the gray trend lines sketched in Figure 1. Assuming that peak eBE in each case corresponds to the vertical detachment energy, this trend suggests that upon solvation core isomer II (ONNNO^-) is stabilized less efficiently than core isomer I (NO^-). The validity of the above assumption should be questioned at small eKEs, where near-threshold effects on photodetachment cross sections skew the observed peak positions away from the true VDEs, as discussed previously for other systems.^{42,43} Qualitatively, however, less efficient stabilization of isomer II is consistent with more diffuse charge density in ONNNO^- , compared to the smaller NO^- anion.

Second, the intensity of the bands corresponding to an ONNNO^- cluster core is observed to decrease along the solvation series relative to that of the NO^- core. This may also be due in part to the increasing proximity of transition II to $\text{eKE} = 0$ (as photodetachment cross sections tend to decrease with decreasing eKE).^{44,45} However, the eKE effect alone does not appear to be sufficient to account for the rapid decrease in the relative intensity of transition II observed with increasing n . We therefore conclude that the relative population of the ONNNO^- -based clusters decreases with increasing solvation relative to that of the NO^- -based isomers.

Both of these observations suggest that increasing solvation favors, in a thermodynamic sense, the smaller NO^- core. We caution, however, that this interpretation discounts the effect of low eKEs on the photodetachment cross sections. A quantitative discussion of the solvation-dependent energetics of isomer II, properly accounting for the low-eKE effects, requires modeling the partial-wave composition of the photodetached electrons.⁴³ Alternatively, probing isomer II at higher photon energy would minimize the low-eKE effects and yield a more quantitative picture of its solvation energetics.

Putting the present observations in a broader context, a similar behavior was implicated in the $\text{O}^-(\text{N}_2\text{O})_n \leftrightarrow \text{NNO}_2^-(\text{N}_2\text{O})_{n-1}$ cluster series, where a switch from the NNO_2^- to the O^- cluster core occurs at $n = 4$.²¹ In the present case, we argue that more favorable solvation of NO^- , compared to ONNNO^- , results in a gradual decrease in the relative population of the latter, i.e., gradual $\text{ONNNO}^-(\text{N}_2\text{O})_{n-1}$ to $\text{NO}^-(\text{N}_2\text{O})_n$ core-shifting, rather than abrupt core-switching.

Depolarization of Angular Distributions by Photoelectron–Solvent Scattering. We now move on to the solvation effects on the photoelectron angular distributions in the photodetachment of $\text{NO}^-(\text{N}_2\text{O})_n$, $n = 1-7$ (type I transitions in Figure 1) and $\text{O}^-(\text{N}_2\text{O})_n$, $n = 4-9$. The anisotropy values (β) for the two cluster series, derived from the present work as well as past measurements,^{8,21} are plotted in Figure 2a,b, respectively, as functions of eKE. The following analysis closely follows the procedure outlined previously.⁸

In examining the angular distributions in photodetachment of cluster anions, it is instructive to separate the effects of solvation on the initial and final states of the detached electron from pure kinetic-energy effects. Namely, solvation-induced changes in eKE for a given transition (as indicated, for example, by the band shifts in Figure 1) are presumed to affect partial-wave composition of the photoelectrons in the same way as a red shift of the detachment wavelength would. The resulting anisotropy variation can be described approximately using the Bethe⁴⁶ and Cooper–Zare³⁻⁵ central-potential model, assuming Wigner scaling of partial-wave cross sections.^{34,44} This variation is purely eKE-induced and does not reflect the solvent-induced perturbation of the initial- or final-state wave functions. In this paradigm, the Cooper–Zare curve $\beta_{\text{cz}}(\text{eKE})$ provides a zero-solvation reference, which describes pure eKE effects on anisotropy, while discounting such effects as photoelectron–solvent scattering and perturbation of the shape of the parent electron orbital.

The solid curves in Figure 2a,b are obtained by fitting the Cooper–Zare model equation³⁻⁵ under the Wigner approximation⁴⁴ to the experimental data for bare NO^- (with effective $l = 2$) and O^- ($l = 1$), respectively. The model uses two fitting parameters: A , related to the spatial extent of the negative ion, and φ , the relative phase of the $l \pm 1$ partial waves.³⁻⁵ The O^- curve in Figure 2b has been well-studied and our data for unsolvated O^- are fit well over the entire energy range using the previously reported values of $A = 0.55 \text{ eV}^{-1}$ and $\cos \varphi = 0.96$,^{34,47} with respective standard errors of 0.045 and 0.053. The resulting curve closely matches the curve first computed by Cooper and Zare.³ The NO^- curve in Figure 2a has been adjusted relative to that used previously⁸ to fit the new 266 nm data. The new fit parameter values used in Figure 2a are $A = 0.336 \text{ eV}^{-1}$ and $\cos \varphi = 0.896$, obtained via a nonlinear regression with respective standard errors of 0.031 and 0.039. The old values of $A = 0.383 \text{ eV}^{-1}$ and $\cos \varphi = 0.881$ are well within two standard errors of the new fit and the adjustment does not appreciably affect the analysis or conclusions of this or the previous work.

The effects of solvent-induced perturbations of the final and initial photoelectron wave functions can now be quantified by calculating the difference between the experimental β values for cluster anions and the Cooper–Zare predictions for the unsolvated core anions at the observed transition’s peak eKE. When the results for clusters of different sizes are compared, the difference between the experimental values, $\beta(\text{eKE})$, and the Cooper–Zare predictions, $\beta_{\text{cz}}(\text{eKE})$, should be normalized by the corresponding degree of solvation. Since the cumulative

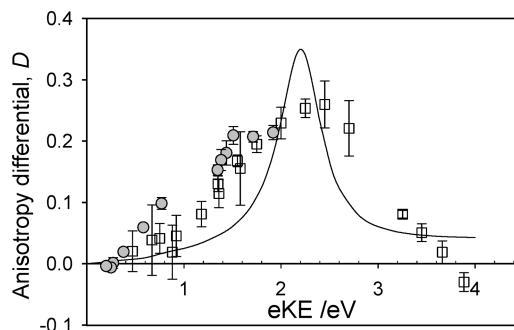


Figure 4. Anisotropy differentials $D(\text{eKE})$, calculated according to eq 1 for $\text{NO}^-(\text{N}_2\text{O})_n$ (open squares) at 786 nm ($n = 1-3$), 532 nm ($n = 1-5$), 355 nm ($n = 1-7$), and 266 nm ($n = 1-4$), and for $\text{O}^-(\text{N}_2\text{O})_n$ (gray circles) at 355 and 266 nm ($n = 4-9$). Error bars correspond to ± 2 standard deviations. The computed $^2\Pi$ momentum-transfer cross-section for electron- N_2O scattering¹⁵ is also plotted with arbitrary scaling relative to $D(\text{eKE})$.

effect of several solvent molecules is not expected to scale linearly with n , an empirical scaling exponent is introduced, as described in the previous publication,⁸ giving rise to the normalized solvent-induced anisotropy differential $D(\text{eKE})$ defined by eq 1.

The deviations of the $\text{NO}^-(\text{N}_2\text{O})_n$ and $\text{O}^-(\text{N}_2\text{O})_n$ photoelectron anisotropies from the corresponding NO^- and O^- Cooper–Zare curves are most pronounced at $\text{eKE} \sim 2 \text{ eV}$ (see Figure 2). The $D(\text{eKE})$ values for both the $\text{NO}^-(\text{N}_2\text{O})_n$ and $\text{O}^-(\text{N}_2\text{O})_n$ cluster series, including all available cluster sizes and wavelengths studied, are plotted in Figure 4. Note that the anisotropy differentials for the O^- -based clusters fall close to those for the NO^- -based clusters for comparable eKEs. We also note that adjusting the phase parameter in the O^- Cooper–Zare curve (using, for example, $\cos \varphi = 0.925$, as used in refs 35 and 47) does not significantly alter the anisotropy differentials for the O^- -based clusters. While the large VDEs of the O^- -based clusters prohibit comparison in the $\text{eKE} = 2-4 \text{ eV}$ range, the overlap between the $\text{NO}^-(\text{N}_2\text{O})_n$ and $\text{O}^-(\text{N}_2\text{O})_n$ anisotropy differentials at $\text{eKE} < 2 \text{ eV}$ is remarkable.

This agreement suggests that the observed anisotropy deviations are not primarily due to the effects of solvation on the core anions, NO^- or O^- . Instead, the trend exhibited by the normalized anisotropy differentials reflects the properties of the solvent, N_2O , which is what the two cluster types studied have in common. The overall $D(\text{eKE})$ dependence, derived from the combination of the $\text{NO}^-(\text{N}_2\text{O})_n$ and $\text{O}^-(\text{N}_2\text{O})_n$ data, mirrors the main trend of the momentum-transfer cross-section⁴⁸ for $\text{N}_2\text{O} + \text{e}^-$ scattering.¹⁵ The corresponding curve, taken from the work of Winstead and McKoy¹⁵ is plotted in Figure 4. The broad $D(\text{eKE})$ maximum is near 2.4 eV, quite close to the $^2\Pi$ electron- N_2O scattering resonance peaking at 2.25 eV.¹⁵ The broader width of the $D(\text{eKE})$ curve compared to that of the resonance is likely due to the spread in effective energies of the photoelectrons undergoing scattering interaction with the solvent.⁴⁹ As discussed previously,⁸ the effective “near-field” energy of this interaction, while difficult to quantify, is expected to differ appreciably from the “far-field” eKE measured in the experiment.

Resonant Repolarization of Photoelectron Angular Distributions? The foregoing discussion demonstrates that the observed solvent-induced decrease in photoelectron anisotropy magnitude may be attributed to scrambling of photoelectron angular distributions due to interaction with solvent molecules. Such scrambling appears to be particularly effective in the presence of solvent-based anionic resonances.^{8,12} We now

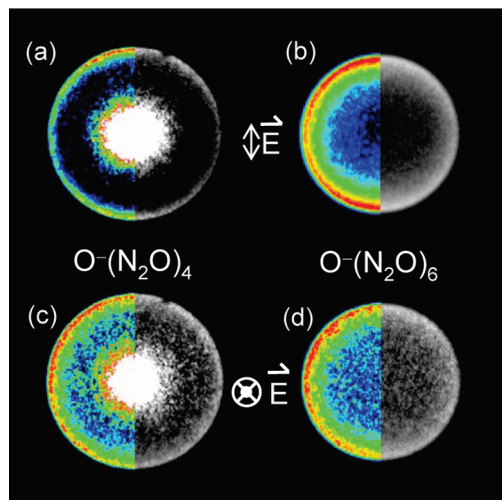


Figure 5. Representative photoelectron images for $\text{O}^-(\text{N}_2\text{O})_n$ at 266 nm with the laser polarized parallel [(a) $n = 4$ and (b) $n = 6$] and perpendicular [(c) $n = 4$ and (d) $n = 6$] to the plane of the detector. Images are shown in split scales arbitrarily chosen to assist in comparison.

consider the possibility that a scattering resonance not only may depolarize (scramble) a photoelectron's angular distribution but also may in fact *repolarize* it in a different direction. To do so, we turn to another observation from the 266 nm $\text{O}^-(\text{N}_2\text{O})_n$ anisotropy values.

As seen in Figure 2b, the 266 nm β values in the eKE = 1.3–1.9 eV range not only deviate very strongly from the values expected in the photodetachment of bare O^- but are also *opposite in sign*, all ranging between 0 and +0.12. To stress this point, the raw photoelectron images for two selected clusters, $\text{O}^-(\text{N}_2\text{O})_4$ and $\text{O}^-(\text{N}_2\text{O})_6$, are shown in Figure 5a,b and their slightly positive anisotropy is apparent even by visual inspection. The analysis yields β values of 0.08 ± 0.04 and 0.12 ± 0.06 for $\text{O}^-(\text{N}_2\text{O})_4$ and $\text{O}^-(\text{N}_2\text{O})_6$, respectively, with ± 2 standard deviations reported, also shown as the error bars in Figure 2b.

In view of the unexpected nature of this result, we tested for the possibility that the sign change is due to a systematic error in our imaging system. Additional measurements on these two species were carried out with the laser polarization aligned in the direction perpendicular to the plane of the detector, collecting photoelectron signals for 150 000 experimental cycles (with corresponding background subtraction). In this configuration, the photoelectron angular distribution should appear isotropic in the image plane, regardless of the nature of the transition probed. This is confirmed by visual inspection of the images shown in Figure 5c,d and the anisotropy parameters obtained upon their reconstruction³¹ (-0.005 and $+0.007$, respectively), both well within the confidence limits of the expected $\beta = 0$ value.

Therefore, although the magnitudes of the proper $\text{O}^-(\text{N}_2\text{O})_n$ 266 nm anisotropy values in Figure 2b are small, the above test suggests that their sign is in fact significant. The change in the apparent character of cluster photodetachment transitions may mean that an accessible scattering resonance has the capacity to *repolarize* a photoelectron.

The lifetime of the resonance is ~ 1 fs.⁵⁰ Considering the time scales of electronic motions (hundreds of attoseconds),⁵¹ this lifetime may be sufficient to completely scramble the original angular distribution. However, this view does not necessarily imply that electrons passing through a resonance are re-emitted

isotropically. In fact, in the $\text{N}_2\text{O} + e^-$ case, the electrons were both predicted¹⁵ and observed⁵² to scatter with a p-like distribution polarized preferentially in the backward and forward scattering directions. Applying this result to cluster–anion photodetachment requires not only explicit knowledge of the cluster's geometry but also the phase shifts associated with scattering events, which may result in new interference effects.

We thus hypothesize that photoelectrons resonantly scattered by solvent molecules, though stripped of their nascent angular distributions, will not necessarily have completely isotropic final angular distributions. In the absence of complete scrambling, the final distribution's character may be determined by the cluster geometry and specific details of the solvent-based resonance. In this light, the fact that the above observation of possible photoelectron repolarization is made for the $\text{O}^-(\text{N}_2\text{O})_n$ cluster anions, but not for $\text{NO}^-(\text{N}_2\text{O})_n$, is likely due to differences in the geometric structures and the solvation numbers of the two cluster types studied.

5. Conclusions

We have discussed the effect of solvation by N_2O on photodetachment from O^- and NO^- . In both cases, the photoelectron anisotropy parameters deviate strongly from the corresponding zero-solvation reference curves. The solvation-number-scaled anisotropy differentials $D(\text{eKE})$ for the O^- -based clusters follow the same trend as those for the clusters with NO^- cores (at least in the eKE-range common for the two data sets). These results suggest that the observed anisotropy effects are dictated predominantly by the identity of the solvent, rather than the anionic cluster core, as it is the solvent that the $\text{O}^-(\text{N}_2\text{O})_n$ and $\text{NO}^-(\text{N}_2\text{O})_n$ cluster anion series have in common. Further, the scaled anisotropy differentials peak in the vicinity of the known electron– N_2O $^2\Pi$ scattering resonance. While the trend in $D(\text{eKE})$ is broadened relative to the momentum-transfer cross-section for electron– N_2O scattering, the qualitative similarity is quite apparent, especially considering that the scattering process is expected to be affected by the cluster environment. We therefore conclude that the solvation effect on the photoelectron angular distributions in these cases is primarily due to resonant interaction of photoelectrons with the N_2O solvent, rather than a solvent-induced perturbation of the parent-anion electronic wave function.

Additionally, photoelectron anisotropy parameters for 266 nm detachment from O^- under N_2O solvation appear to be slightly positive, opposite in sign to the expected values for detachment from bare O^- in the same eKE-range. The corresponding data points fall close in energy to the electron– N_2O scattering resonance. If this observation is indeed due to resonant photoelectron–solvent scattering, one possible explanation is that autodetachment from the N_2O^- resonance state is not necessarily isotropic. This explanation is consistent with the p-type (forward–backward) nature of the $e^- + \text{N}_2\text{O}$ scattering interaction in the vicinity of the $^2\Pi$ resonance.

Further studies of the effects of solvation on photoelectron anisotropy move us toward a more detailed understanding of photodetachment and the extent to which we can learn from photoelectron anisotropy measurements. Resonant photoelectron–solvent scattering may also have implications for modeling and understanding photoinduced electron-transfer dynamics.

Acknowledgment. This work is supported by the National Science Foundation (grant CHE-0713880).

References and Notes

- (1) Ervin, K. M.; Lineberger, W. C. Photoelectron Spectroscopy of Negative Ions. In *Advances in Gas Phase Ion Chemistry*; Adams, N. G., Babcock, L. M., Eds.; JAI Press: Greenwich, CT, 1992; Vol. 1, p 121.
- (2) Sanov, A.; Mabbs, R. *Int. Rev. Phys. Chem.* **2008**, *27*, 53.
- (3) Cooper, J.; Zare, R. N. *J. Chem. Phys.* **1968**, *48*, 942.
- (4) Cooper, J.; Zare, R. N. *J. Chem. Phys.* **1968**, *49*, 4252.
- (5) Cooper, J.; Zare, R. N. Photoelectron angular distributions. In *Atomic collision processes*; Geltman, S., Mahanthappa, K. T., Brittin, W. E., Eds.; Gordon and Breach, Science Publishers: New York, London, Paris, 1968; Vol. XI-C, p 317.
- (6) Surber, E.; Mabbs, R.; Sanov, A. *J. Phys. Chem. A* **2003**, *107*, 8215.
- (7) Mabbs, R.; Grumbling, E. R.; Pichugin, K.; Sanov, A. *Chem. Soc. Rev.*, in press.
- (8) Velarde, L.; Habteyes, T.; Grumbling, E. R.; Pichugin, K.; Sanov, A. *J. Chem. Phys.* **2007**, *127*, 084302.
- (9) Castleman, A. W.; Bowen, K. H. *J. Phys. Chem.* **1996**, *100*, 12911.
- (10) Sanov, A.; Lineberger, W. C. *Phys. Chem. Chem. Phys.* **2004**, *6*, 2018.
- (11) Arnold, D. W.; Bradforth, S. E.; Kim, E. H.; Neumark, D. M. *J. Chem. Phys.* **1992**, *97*, 9468.
- (12) Mabbs, R.; Surber, E.; Sanov, A. *J. Chem. Phys.* **2005**, *122*, 054308.
- (13) Benitez, A.; Moore, J. H.; Tossell, J. A. *J. Chem. Phys.* **1988**, *88*, 6691.
- (14) Nakanishi, R.; Muraoka, A.; Nagata, T. *Chem. Phys. Lett.* **2006**, *427*, 56.
- (15) Winstead, C.; McKoy, V. *Phys. Rev. A* **1998**, *57*, 3589.
- (16) Hiraoka, K.; Fujimaki, S.; Aruga, K.; Yamabe, S. *J. Phys. Chem.* **1994**, *98*, 8295.
- (17) Resat, M. S.; Zengin, V.; Garner, M. C.; Continetti, R. E. *J. Phys. Chem. A* **1998**, *102*, 1719.
- (18) DeLuca, M. J.; Niu, B.; Johnson, M. A. *J. Chem. Phys.* **1988**, *88*, 5857.
- (19) Tsukuda, T.; Johnson, M. A.; Nagata, T. *Chem. Phys. Lett.* **1997**, *268*, 429.
- (20) Shin, J. W.; Hammer, N. I.; Johnson, M. A.; Schneider, H.; Gloss, A.; Weber, J. M. *J. Phys. Chem. A* **2005**, *109*, 3146.
- (21) Pichugin, K.; Grumbling, E.; Velarde, L.; Sanov, A. *J. Chem. Phys.* **2008**, *129*, 044311.
- (22) Eppink, A. T. J. B.; Parker, D. H. *Rev. Sci. Instrum.* **1997**, *68*, 3477.
- (23) Parker, D. H.; Eppink, A. T. J. B. *J. Chem. Phys.* **1997**, *107*, 2357.
- (24) Chandler, D. W.; Houston, P. L. *J. Chem. Phys.* **1987**, *87*, 1445.
- (25) Heck, A. J. R.; Chandler, D. W. *Annu. Rev. Phys. Chem.* **1995**, *46*, 335.
- (26) Thoman, J. W.; Chandler, D. W.; Parker, D. H.; Janssen, M. H. M. *Laser Chem.* **1988**, *9*, 27.
- (27) Eland, J. H. D. *Photoelectron spectroscopy: an introduction to ultraviolet photoelectron spectroscopy in the gas phase*; Butterworths: London, 1984.
- (28) Johnson, M. A.; Lineberger, W. C. Pulsed Methods for Cluster Ion Spectroscopy. In *Techniques for the Study of Ion Molecule Reactions*; Farrar, J. M., Saunders, W. H., Eds.; Wiley: New York, 1988; p 591.
- (29) Robertson, W. H.; Kelley, J. A.; Johnson, M. A. *Rev. Sci. Instrum.* **2000**, *71*, 4431.
- (30) Wiley, W. C.; McLaren, I. H. *Rev. Sci. Instrum.* **1955**, *26*, 1150.
- (31) Dribinski, V.; Ossadtchi, A.; Mandelshtam, V. A.; Reisler, H. *Rev. Sci. Instrum.* **2002**, *73*, 2634.
- (32) Coe, J. V.; Snodgrass, J. T.; Friedhoff, K. M.; Bowen, K. H. *J. Chem. Phys.* **1987**, *87*, 4302.
- (33) Hendricks, J. H.; de Clercq, H. L.; Freidhoff, C. B.; Arnold, S. T.; Eaton, J. G.; Fancher, C.; Lyapustina, S. A.; Snodgrass, J. T.; Bowen, K. H. *J. Chem. Phys.* **2002**, *116*, 7926.
- (34) Hanstorp, D.; Bengtsson, C.; Larson, D. J. *Phys. Rev. A* **1989**, *40*, 670.
- (35) Snis, A.; Panas, I. *Chem. Phys. Lett.* **1999**, *305*, 285.
- (36) Alijah, A.; Kryachko, E. S. *J. Mol. Struct.* **2007**, *844*, 193.
- (37) Kryachko, E. S.; Vinckier, C.; Nguyen, M. T. *J. Chem. Phys.* **2001**, *114*, 7911.
- (38) Pichugin, K.; Goebbert, D.; Grumbling, E. R.; Sanov, A. Unpublished results.
- (39) Ervin, K. M.; Ho, J.; Lineberger, W. C. *J. Phys. Chem.* **1988**, *92*, 5405.
- (40) Weaver, A.; Metz, R. B.; Bradforth, S. E.; Neumark, D. M. *J. Chem. Phys.* **1989**, *90*, 2070.
- (41) Luong, A. K.; Clements, T. G.; Continetti, R. E. *Int. J. Mass Spectrom.* **2002**, *220*, 253.
- (42) Surber, E.; Sanov, A. *J. Chem. Phys.* **2002**, *116*, 5921.
- (43) Surber, E.; Sanov, A. *J. Chem. Phys.* **2003**, *118*, 9192.
- (44) Wigner, E. P. *Phys. Rev.* **1948**, *73*, 1002.
- (45) Lineberger, W. C.; Hotop, H.; Patterson, T. A. Photodetachment Threshold Processes. In *Electron and Photon Interactions with Atoms*; Kleinpoppen, H.; McDowell, M. R. C., Eds.; Plenum Publishing Corp.: New York, 1976; p 125.
- (46) Bethe, H. A. *Handbuch Phys.* **1933**, *24*, 483.
- (47) Cavanagh, S. J.; Gibson, S. T.; Gale, M. N.; Dedman, C. J.; Roberts, E. H.; Lewis, B. R. *Phys. Rev. A* **2007**, *76*, 052708.
- (48) *Electron-Molecule Collisions*; Shimamura, I., Takahashi, K., Eds.; Plenum Press: New York, 1984; p 570.
- (49) Hanel, G.; Fiegele, T.; Stamatovic, A.; Mark, T. D. *Int. J. Mass Spectrom.* **2001**, *205*, 65.
- (50) Dube, L.; Herzenberg, A. *Phys. Rev. A* **1975**, *11*, 1314.
- (51) Uiberacker, M.; Uphues, T.; Schultze, M.; Verhoef, A. J.; Yakovlev, V.; Kling, M. F.; Rauschenberger, J.; Kabachnik, N. M.; Schroder, H.; Lezius, M.; Kompa, K. L.; Muller, H. G.; Vrakking, M. J. J.; Hendel, S.; Kleineberg, U.; Heinzmann, U.; Drescher, M.; Krausz, F. *Nature* **2007**, *446*, 627.
- (52) Kitajima, M.; Sakamoto, Y.; Watanabe, S.; Suzuki, T.; Ishikawa, T.; Tanaka, H.; Kimura, M. *Chem. Phys. Lett.* **1999**, *309*, 414.